Title Developmental and Early-Life Stress-Induced Effects on 5-HT_3R-Expressing Interneurons within Auditory Cortex

Authors James T. Moore [1,2], Matthew J. Sunthimer [1,2], Ethan White [1], Jeffrey G. Mellott [1,3,4], and Merri J. Rosen [a,1,3,4]

Affiliations

[1)] Hearing Research Group
Department of Biomedical Sciences
Northeast Ohio Medical University
Rootstown, OH, USA

[2)] Biomedical Sciences Program
Kent State University
Kent, OH, USA

[3)] University Hospitals | NEOMED Hearing Research Center
Northeast Ohio Medical University
Rootstown, OH, USA

[4)] Brain Health Research Institute
Kent State University
Kent, OH, USA

[a)] Corresponding author: mrosen@neomed.edu

Keywords development, early-life stress, adversity, auditory cortex, serotonin, 5-HT3R, layer 1, inhibition, critical period

Figures: 4
Tables: 2
Word Count:

Abstract	239
Introduction	793
Discussion	2007

Competing Interests

The authors declare no competing interests.

Acknowledgements

This work was supported by NIDCD R01 DC013314 to MJR, NIDCD R01 supplement DC013314-09S1 to JTM, and NIDCD R01 DC017708 to JGM. The content is solely the responsibility of the authors and does not necessarily represent the official views of the National Institutes of Health. The authors would like to thank Dr. Jesse W. Young for help with statistical modeling, and Dr. Jeffrey Wenstrup for comments on an earlier version of the manuscript.

ABSTRACT

Early life stress (ELS) is a well-known predictor of neuropsychiatric disease and contributes to the development of sensory processing deficits that persist throughout life. Organisms are particularly susceptible to the deleterious effects of stress during critical periods, when neuroplasticity is heightened, and initial representations of the sensory environment are mapped to cortex. When ELS is induced during the auditory cortical (ACx) critical period, it impairs both neural and behavioral responses to a variety of auditory stimuli that rely on temporal processing. Mechanisms by which ELS may alter critical period plasticity are of particular interest in understanding ELS-related pathology, including the 5-HT3R interneuron system, which has been implicated in regulating neural activity during critical periods. Here we examined two principal subpopulations of interneurons in primary ACx: VIP and NDNF cells, which account for a majority of cortical neurons expressing 5-HT3R. The expression of the Htr3a gene during normal development and under ELS conditions was quantified using multiplex fluorescent in situ hybridization. We show that densities of cells expressing NDNF and VIP decrease following ear opening and across the ACx critical period, and that ELS results in the maintenance of elevated cell densities compared to age-matched controls. Further, Htr3a in VIP neurons is developmentally upregulated, and its expression is further increased by ELS beyond normal physiologic levels. Stress-induced shifts in these serotonergic interneurons may contribute to deficits that arise in auditory cortical and perceptual responses via effects on local cortical circuitry.

INTRODUCTION

Early life stress (ELS) contributes to neuropsychiatric disease in both humans and animal models (Kessler et al., 2010; Chen and Baram, 2016; Yajima et al., 2018). Emotional and cognitive regions of the brain are particularly susceptible to insults from stress during 'critical periods': distinctive time windows of heightened plasticity where susceptibility to early adverse experiences is maximal (Dunn et al., 2019; Gabard-Durnam and McLaughlin, 2019; Malave et al., 2022). Recent investigations of ELS have broadened beyond emotional and cognitive regions to include sensory cortices, indicating that ELS can directly disrupt sensory processing (Takatsuru and Koibuchi, 2015; Liu et al., 2020; Ye et al., 2023; Poplawski et al., 2024; An et al., 2025; Mazi et al., 2025; Rosen and Huyck, 2025). When ELS is induced during the auditory cortical (ACx) critical period, it impairs both neural and behavioral responses to a variety of auditory stimuli that rely on temporal processing, such as accurate detection of brief gaps in sound, frequency modulations, and sound locations (Ye et al., 2023; An et al., 2025; Mazi et al., 2025). Mechanistically, these deficits are accompanied by reductions in several cortical elements known to be involved in critical period plasticity: inhibitory parvalbumin neurons (PV), perineuronal nets (PNNs), and brain-derived neurotrophic factor (BDNF) (Bath et al., 2013; Takesian and Hensch, 2013; Castillo-Gomez et al., 2017; Murthy et al., 2019; Guadagno et al., 2021; Sunthimer et al., 2023; An et al., 2025; Mazi et al., 2025). An important player that has received less attention is serotonin (5-HT).

Serotonin is linked to stress, developmental plasticity, and the auditory system. Serotonergic neurons project to ACx and other auditory regions, releasing serotonin based on behavioral contexts including stress (Campbell et al., 1987; DeFelipe et al., 1991; Clement et al., 1998; Kranz et al., 2010; Hurley and Hall, 2011; Koyama et al., 2017). Stress can induce widespread effects on the serotonergic system, altering levels of 5-HT and 5-HT receptors (5-HTRs) throughout the brain (Veenema, 2009; Bravo et al., 2014; Lages et al., 2021). Within the auditory system, such serotonergic shifts can affect neural excitability (Lee et al., 2010; Rao et al., 2010), sound-evoked response properties (Hurley and Pollak, 2005; Hall et al., 2010; Cheng et al., 2023b; Horrocks et al., 2025), and behavioral responses to sound (Adler et al., 2005; Tsitsipa et al., 2022). Serotonergic effects are pronounced during early postnatal development, where manipulations that increase 5-HT levels cause later behavioral hypersensitivity to sound and disruption of ACx sound-evoked response properties (Kahne et al., 2002; Simpson et al., 2011; Pan et al., 2021). Such early susceptibility suggests a role for 5-HT during critical period plasticity. Indeed, blocking 5-HT activity reduces plasticity in prefrontal, somatosensory, and visual cortices specifically during critical periods involving those regions (Cases et al., 1996; Wang et al., 1997; Rebello et al., 2014). Even in humans, increasing 5-HT levels perinatally via serotonin reuptake inhibitors accelerates the maturation of speech perception in infants (Weikum et al., 2012).

Within ACx, superficial interneurons that express 5-HT3 receptors (5-HT3R) may have a role in regulating critical period plasticity. These cells integrate bottom-up auditory information with top-down neuromodulatory input, responding to sound with response properties that are modulated by behavioral state (Sweeney et al., 2025; Vattino et al., 2025). Optogenetic inactivation of 5-HT3R cells during the ACx critical period eliminates tonotopic map plasticity in A1, demonstrating their involvement in experience-

86 dependent developmental plasticity (Takesian et al., 2018). Converging lines of research also suggest that
87 ELS affects 5-HT3R gene expression. In rats, 5-HT3aR mRNA levels were increased by ELS in prefrontal
88 cortex and hippocampus (Zolfaghari et al., 2021), and in psychiatric patients, childhood maltreatment was
89 associated with epigenetic changes in the gene encoding 5-HT3R (Perroud et al., 2016).

90 The extent to which 5-HT3R expression contributes to critical period plasticity or to altered circuit
91 dynamics resulting from ELS is currently limited by a lack of detailed information concerning the native
92 expression profiles of 5-HT3R within the two major subpopulations of 5-HT3R cells: vasoactive intestinal
93 peptide (VIP) cells that are densely populated in superficial cortical layers, and neuron derived
94 neurotrophic factor (NDNF) cells that are mostly confined to L1 (Kullander and Topolnik, 2021; Hartung et
95 al., 2024). Both groups innervate a combination of other interneurons and dendrites of pyramidal cells to
96 form complex disinhibitory circuits that are involved in gating cortical responses and guiding
97 neuroplasticity (Donato et al., 2013; Takesian et al., 2018; Hartung et al., 2024) (Figure 1A). Here, we
98 characterized the cell type-specific expression profiles of the Htr3a gene in these cells within A1 during
99 normal development and under the influence of ELS. This revealed that Htr3a is differentially expressed
100 between NDNF and VIP cell types in a layer-specific manner. Further, ELS affects both cell density and
101 Htr3a expression levels, potentially causing long-term alterations to cortical function and neuroplasticity.

102 MATERIALS AND METHODS

103 *Subjects*

104 All experiments followed procedures approved by the Northeast Ohio Medical University Institutional
105 Animal Care and Use Committee. Mixed-sex groups of Mongolian gerbils (*Meriones unguiculatus)* were
106 used, as they are an established animal model for the study of auditory processing. Gerbils from multiple
107 litters were housed with littermates in a 12/12 h light/dark cycle and fed ad libitum. Control and ELS
108 animals were collected from separate litters to avoid stressful effects on control animals or parents
109 induced by removing siblings for ELS treatment.

110 *Experimental Design*

111 Development of $NDNF^+$ and VIP^+ cell populations was examined by sampling brain sections containing
112 A1 from five animal groups (Figure 1B). We performed mRNA *in situ* hybridization in three channels
113 simultaneously, using custom probes targeting *NDNF*, *VIP*, and *Htr3a.* Control animals were sacrificed at
114 postnatal day (P)10 and P15 to characterize a timeline of normal development in A1 during the ACx critical
115 period, which occurs approximately from ear canal opening ~P11 through P23 (Mowery et al., 2015). A
116 third control group was sacrificed at P30 following closure of the critical period. Two ELS groups,
117 "Restraint" ELS (ELS_R) and "Open field" ELS (ELS_O) were subjected to separate forms of stress induction
118 during the ACx critical period as described below, and sacrificed at P30 to elucidate the residual effects of
119 ELS on A1 development. All groups contained 6 subjects: P15 controls (CTR15's) contained 4 males and 2
120 females; P30 controls (CTR30's) contained 2 males and 4 females; all other groups were balanced equally
121 by sex. For each group, three measures were quantified: 1) Cell population density within each layer of A1

122 for *NDNF* and *VIP*-labeled cells, 2) number of *Htr3a* mRNA within each NDNF and VIP cell, and 3) number of
123 NDNF puncta within each NDNF cell.

124 *Stress Induction*

125 ELS_R animals were subjected to intermittent sessions of maternal separation and restraint across a 16-
126 day time window encompassing the critical period for maturation of ACx intrinsic and synaptic properties
127 (Mowery et al., 2015). This corresponded to P9-P24 and consisted of ten 2-h restraint sessions occurring in
128 the morning, afternoon, or evening. Time of day was varied randomly to reduce predictability in order to
129 increase stress (Baram et al., 2012). During each session, animal cages were transported from the animal
130 facility to a testing room, where the pups were removed and placed into 50-ml centrifuge tubes isolated
131 from their parents and littermates. The tubes were perforated to allow easy breathing and placed either
132 vertically or horizontally inside sound attenuated, anechoic booths with lights on. Pups were returned to
133 their home cage and then to the animal facility immediately following each session.

134 ELS_O animals were subjected to intermittent sessions of maternal separation and isolation in open
135 spaces during a 9-day time window corresponding to P11-P19, consisting of six 2-h open isolation sessions
136 occurring in the morning, afternoon, or evening. The ELS_O group received fewer isolation sessions over a
137 compacted developmental time window compared to the ELS_R group. These parameters were chosen to
138 span the developmental time window of maximal plasticity while avoiding malnutrition and neglect,
139 because using the timing of ELS_R isolation in the ELS_O paradigm resulted in reduced body weight (data
140 not shown). Pups were separated from their home cage and transported to a testing room where they
141 were placed individually into 10.5" x 12.5" clear acrylic boxes with no bedding or environmental stimuli.
142 The boxes were then placed into sound attenuated, anechoic booths with lights off. Pups were returned
143 to the animal facility and back to their original home cage immediately following each session.

144 *RNA fluorescent in situ hybridization (FISH)*

145 Gerbils at P10, P15, or P30 were anaesthetized with isoflurane and decapitated. Brains were rapidly
146 removed, embedded in Optimal Cutting Temperature medium (OCT, Scigen) and flash frozen. 14µm
147 coronal sections containing A1 were then collected on a cryostat microtome (Leica CM 1950) and adhered
148 to SuperFrost Plus slides (Fisher Scientific). Sections were chosen based on anatomical landmarks
149 corresponding to Plates 30-32 from the brain atlas of the Mongolian gerbil (Radtke-Schuller et al., 2016).
150 These landmarks included the presence of lateral ventricles lateral to the thalamus, and hippocampus
151 expanding dorsoventrally. Sections were chosen to be anterior to the superior collicus and taken from
152 the widest portion of the brain measured medio-laterally. Slides were stored under airtight conditions at -
153 80°C until use. *In situ* hybridization was performed using the RNAscope Multiplex Fluorescent Reagent Kit
154 v2 (ACDBio) according to manufacturer instructions. Briefly, slides were post-fixed for 1 hour in buffered
155 formalin, dehydrated in a series of ethanol baths (50%,70%, 100%, 100%), then pre-processed with
156 hydrogen peroxide (10 minutes) followed by protease IV (30 minutes). RNAscope probes were hybridized
157 at 40°C for 2 hours, then conjugated to a series of signal-amplifying molecular scaffolds, followed by
158 fluorescent labeling using channel-specific horseradish peroxidases and TSA vivid fluorophores in 1:1500

159 dilution (Tocris). The probes used were as follows: Mun-Htr3a-C1(Cat. #1299361-C1), Mun-Ndnf-C2(Cat.
160 #1299341-C2), and Mun-Vip-C3(Cat. #1299351-C3). All slides were counterstained with DAPI for 30s prior to
161 coverslipping with Prolong Gold antifade mountant (Invitrogen).

162 *Imaging and Cell Quantification*

163 Data for VIP$^+$ cells were collected from a single tissue section from each subject. In addition to the
164 primary tissue section, NDNF$^+$ data were also collected from a second section, when available, to ensure
165 sufficient sampling due to their lower abundance. A1 was identified using thalamic and hippocampal
166 anatomical landmarks guided by the gerbil brain atlas (Figure 1C; Radtke-Schuller et al., 2016). The dorsal
167 extent of A1 lies near the level of the dentate gyrus (DG); the region extends ventrally to a point just
168 inferior of the lateral pole of cortex in Mongolian gerbils, ~1-2mm superior to the rhinal fissure. We
169 sampled a conservative area extending 2mm along the D-V axis from the level of DG, extending ventrally
170 to just superior of the lateral pole. Both cell populations were sampled throughout neocortical layers 1-4
171 (L1, L2/3 and L4), where the majority of cortical 5HT3R interneurons are concentrated and have been best
172 characterized in the existing literature (Lee et al., 2010; Kullander and Topolnik, 2021). Layers were
173 identified visually based on packing densities illuminated by DAPI, including the koniocortical patterning
174 of L4 seen in primary sensory areas (Radtke-Schuller et al., 2016). Tiled images of A1 containing L1-L4 were
175 taken at 40x in four channels to generate A1 "maps" which were used to identify all cells that expressed
176 *NDNF* or *VIP* mRNA within the region of interest (Figure 1D). We only counted cells that showed at least 2
177 puncta tagged with *NDNF* (NDNF$^+$) or *VIP* (VIP$^+$) label that were localized to an intact DAPI-stained
178 nucleus. Cells with splintered nuclei were likely either damaged by sectioning or programmed cell death
179 and were not counted. Because NDNF is also expressed in epithelial structures such as blood vessels,
180 presumably in non-neuronal cells (Ohashi et al., 2014), NDNF$^+$ cells that were touching the pial surface in
181 L1 or embedded within apparent blood vessels were excluded from analysis (Figure 1E, *blue inset*). The A1
182 maps were subsequently used to draw layer boundaries and record area measurements using the open-
183 source software Fiji (Schindelin et al., 2012) to assess layer distribution. Within each layer, and cell
184 density. All imaging was performed on a Zeiss Axio Imager M2 fluorescent microscope using the
185 accompanying ZEN Blue software. Photos were taken using a Hamamatsu model C13440 digital camera.

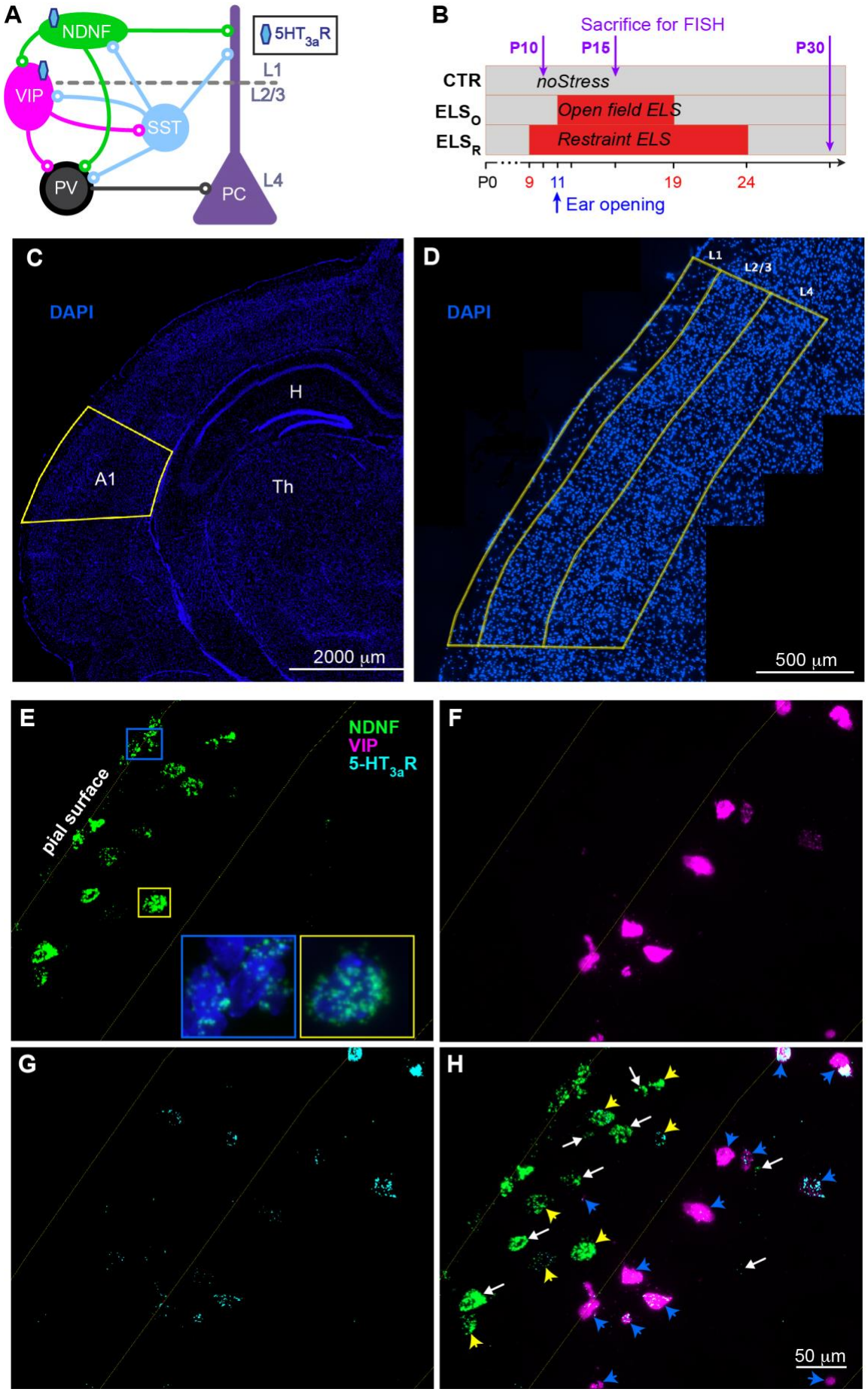
A
NDNF
VIP
SST
PV
PC
5HT3aR
L1
L2/3
L4
B
Sacrifice for FISH
P10
P15
P30
CTR
noStress
ELSO
Open field ELS
ELSR
Restraint ELS
P0
9
11
19
24
Ear opening
C
DAPI
H
A1
Th
2000 µm
D
DAPI
L1
L2/3
L4
500 µm
E
NDNF
VIP
5-HT3aR
pial surface
F
G
H
50 µm

186

Figure 1: Summary of methods. (A) Simplified schematic of NDNF$^+$ and VIP$^+$ connectivity in ACx showing relationships to parvalbumin (PV) and somatostatin (SST) interneurons and pyramidal cells (PC). (B) Timeline of stress induction with endpoints denoting tissue collection. (C) A representative coronal section imaged at 5x in the DAPI channel identifying A1. (D) Tiled image of A1 sampling area taken at 40x, delineating L1, 2/3 and 4. (E-G) Separate fluorescent channels showing target probes for *NDNF*, *VIP* and *Htr3a.* Insets show *NDNF* localized to non-neuronal cells in the pial surface [blue outline] and an NDNF+ neuron [yellow outline]. (H) Composite image showing results of multichannel FISH labeling. All counted cells are indicated by arrows or arrowheads. Arrowheads depict cells with *Htr3a* puncta (yellow for NDNF cells, blue for VIP cells). White arrows depict cells with no *Htr3a* puncta (NDNF cells only).

Htr3a Quantification

The RNAscope assay produces discrete fluorescent puncta corresponding to individual mRNA transcripts which were counted to quantify levels of *Htr3a* mRNA expression. Each NDNF$^+$ and VIP$^+$ cell within A1 was imaged at 150x in three channels (e.g. DAPI+*VIP*+*Htr3a*) and photographed using the same exposure times across cases. Both *NDNF* and *VIP* mRNA were highly abundant within cells and used to demarcate cell boundaries. All *Htr3a* puncta contained within these boundaries were manually counted, either by live-counting for low-expressing cells, or from saved images in Fiji for high-expressing cells (>40 puncta per cell). On high-expressing cell images, a standardized rolling ball background subtraction algorithm was performed and brightness/contrast enhanced to ease quantification. A small number of cells were labeled with multiple *Htr3a* puncta without *NDNF* or *VIP* colocalization, possibly corresponding to other categories of 5-HT3R expressing interneurons and were excluded from analysis.

NDNF Quantification

Cellpose 2.0 human-in-the-loop open-source software was used to automatically segment NDNF puncta using a custom-trained machine learning model (Stringer et al., 2021). Each image was first background subtracted using ImageJ (public domain, Image Processing and Analysis in Java). Cellpose segmented these images to identify individual puncta, then clusters of puncta were manually corrected when grouped inaccurately. A subset of cells expressed high levels of NDNF in which individual puncta were indistinguishable from one another (Figure 4A1). These high-expressing cells were categorized as "saturated" and estimated to have 250 puncta per cell. This number was conservatively chosen to match the highest countable puncta in the unsaturated cases.

Statistical Analyses

Cell densities were calculated as the number of labeled cells within the ROI divided by the area of the ROI in square millimeters, calculated separately for each cell type within each layer. Cell densities between groups of animals were then compared using the Mann-Whitney U test.

Cellular data for *Htr3a* mRNA were examined using two approaches. First, cells were pooled within each treatment condition and predictions were tested using a generalized linear mixed-effects regression model (GLMM) with a Poisson error distribution. This was chosen because the response variable (number of puncta) was coded as count data which had a Poisson distribution, with most cells expressing low levels of *Htr3a* puncta and a tail of high expressors. NDNF$^+$ and VIP$^+$ cell populations were analyzed

separately, with independent models generated for ontogeny (CTR10 vs. CTR15 vs. CTR30) and for ELS (CTR30 vs. ELS_O vs. ELS_R), for a total of 4 models. We specified condition and layer as fixed effects in each model, with subject and sex as random effects. Models were fit in R (RStudio Team, 2024) using the add-on packages "lme4" (Bates et al., 2015) and "lmerTest" (Kuznetsova et al., 2017). Type III Wald Chi-Square tests were performed on the factors within each model. Post hoc contrast analyses were performed on resulting estimated marginal means using the add-on package "emmeans" (Lenth, 2023). For multiple comparisons, the Benjamini-Hochberg method was used to identify significant p-values at $p < 0.05$ using a critical value of 0.1. Second, we performed a more conservative analysis of *Htr3a* mRNA data using single animal subject as the unit of analysis. Average *Htr3a* puncta per cell, separated by cell type and layer, were calculated for each animal and subjected to Mann-Whitney U tests to compare developmental trajectories and the effects of ELS.

Cellular data for NDNF puncta quantification were also examined with the two approaches described for *Htr3a* mRNA, using the number of NDNF puncta as the response variable.

Data in text are reported as means ± SEM. In boxplots, purple lines are medians, box edges are 25th and 75th percentiles, and whiskers extend to the most extreme data points excluding outliers.

RESULTS

NDNF and VIP Cell Distributions

Consistent with previous reports, we found no colocalization between *NDNF* and *VIP*, which appear as mutually exclusive markers of these cell populations. Across all cases (30 animals), a total of 1,164 $NDNF^+$ cells were identified, of which 73.5% resided in L1, accounting for approximately 90% of the labeled cells in this layer. In general, VIP^+ cells were far more abundant in cortex, with 2,110 cells identified, 2.9% of them residing in L1, 68.3% in L2/3, and 28.8% in L4. Cells in deeper layers were not quantified, as the majority of cortical 5HT3R interneurons are concentrated in L4 and superficial layers (Lee et al., 2010; Kullander and Topolnik, 2021).

NDNF and VIP Population Densities Decrease During the ACx Critical Period

Both $NDNF^+$ and VIP^+ population densities (# cell bodies/mm^2) declined precipitously between P10 and P30 under control conditions (Figure 2). A Mann-Whitney U test revealed that $NDNF^+$ cell density in L1 was significantly higher in CTR10 (Mean=113.74) compared to CTR15 (M=60.48; U=31, p=0.04113). A less robust decline in L1 $NDNF^+$ cells was seen between CTR15 and CTR30 (M=43.02; U=30, p=0.06494; Figure 2A). No significant group differences were found between developmental ages in L2/3 or L4 $NDNF^+$ cell densities.

VIP^+ cell density in L2/3 was significantly higher in CTR10 than CTR15 (M=78.86; U=36, p=0.002165; Figure 2B). A significant reduction in L2/3 VIP^+ density was also observed between CTR15 and CTR30 (M=54.62; U=31, p=0.04113). In L4, VIP^+ cell density declines significantly between CTR10 (M=82.19) and

CTR15 (M=27.88; *U*=36, *p*=0.002165), but does not differ significantly between CTR15 and CTR30 (M=22.15; *U*=26, *p*=0.2403; Figure 2C). No significant group differences were found for L1 VIP$^+$ cell densities.

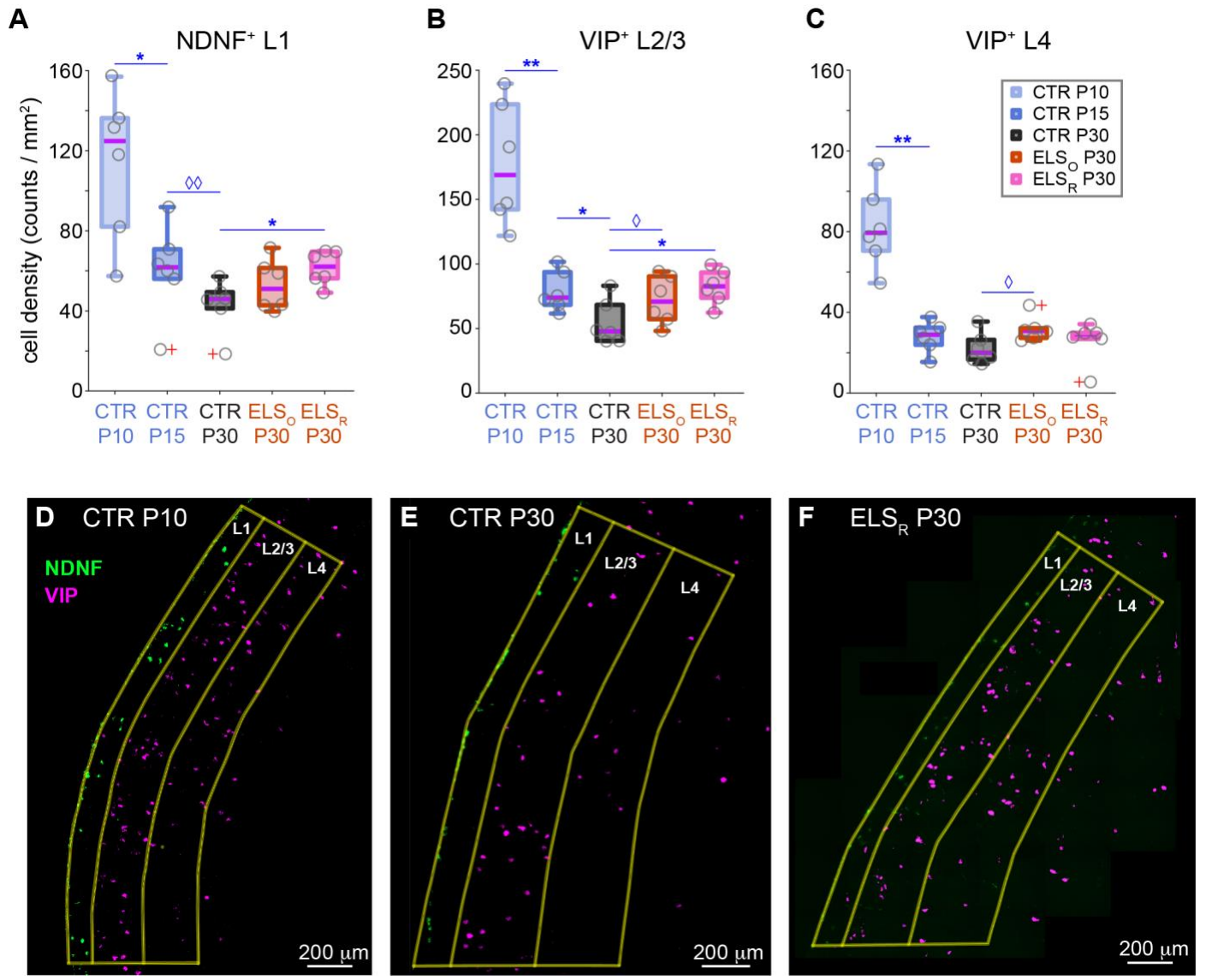

Figure 2: NDNF+ and VIP+ populations drop substantially from P10-P30, but plateau at higher levels under ELS conditions. (A-C) Cell densities within each treatment group; *P* values resulting from pairwise Mann-Whitney U tests (n=6 for all groups). (D-F) Representative A1 maps showing NDNF+ and VIP+ cells for CTR10, CTR30, and ELS$_R$. ****p <0.001, ***p <0.002, **p <0.01, *p <0.05, ◊◊p <0.08, ◊p <0.14. Grey circles in boxplots show individual animal data. Red + symbols inicate outliers.

ELS Attenuates the Decline of NDNF and VIP Population Densities

Cell population densities for both NDNF$^+$ and VIP$^+$ were elevated under ELS conditions compared to age-matched controls at P30 (Figure 2A-C). L1 NDNF$^+$ cell density was significantly higher in RELS animals (M=61.49) compared to P30 Controls (M=43.02; *U*=32, *p*=0.02597). This effect was not statistically significant when ELS$_O$ (M=52.92) were compared to CTR30 (*U*=23, *p*=0.4848). However, the difference was nearly identical to the comparison between ELS$_O$ with CTR15 (M=60.48; *U*=23, *p*=0.4848), suggesting

259 that alterations to the ELS_O phenotype may be present that escape the sensitivity of this test. L1 $NDNF^+$
260 cell density was similar between CTR15 and ELS_R at P30 (U=19, p=0.9372). $NDNF^+$ cell density in L2/3 was
261 also affected by stress, where both ELS_R (M=11.77) and ELS_O (M=10.43) were significantly higher than
262 CTR30 (M=2.83; U=33, p=0.02002; U=34, p=0.01291 for the two comparisons). Within L4, $NDNF^+$ density
263 trended higher in ELS_R (M=4.26) and ELS_O (M=4.97) compared to CTR30 (M=1.66), though this did not
264 reach statistical significance (U=30, p=0.06367 for each).

265 L2/3 VIP^+ cell density was also significantly higher in ELS_R (M=82.34) compared to CTR30 (M=54.62),
266 U=32, p=0.02597. A similar, but less robust trend was seen in ELS_O animals (M=71.95), U=28, p=0.132.
267 Again, neither ELS_R nor ELS_O differed significantly from CTR15 (U=15, p=0.6991; U=22, p=0.5887,
268 respectively). In L4, VIP^+ cell density did not differ significantly between ELS_R (M=25.65) and CTR30, U=25,
269 p=0.3095, while a difference was trending between ELS_O (M=31.78) and CTR30, U=30, p=0.06494. No
270 significant group differences were found for L1 VIP^+ cell densities.

271 *5HT3a mRNA Expression Increases During Normal Development*

272 For all treatment groups, expression of *Htr3a* mRNA skewed low for $NDNF^+$ and VIP^+ cell populations,
273 with a relatively small number of cells containing high concentrations of labeled puncta (Figure 3C-E). In
274 VIP^+ cells, *Htr3a* mRNA expression ranged from 0 to 328 puncta, with over 97% possessing 1 or more per
275 cell. $NDNF^+$ cells demonstrated a considerably lower expression profile, with *Htr3a* puncta per cell
276 ranging from 0 to 137, and almost 23% containing no *Htr3a*.

277 We examined the cell populations pooled within each treatment condition through a GLMM approach
278 using four separate models. In our ontogenetic model of VIP^+ cell development, there was a significant
279 interaction between condition and layer, such that the variance in number of *Htr3a* puncta according to
280 condition depended on layer (Table 1A). Post-hoc tests examining differences between conditions within
281 layers found that L2/3 VIP^+ cells expressed fewer puncta in CTR10 than CTR15, and fewer puncta in CTR15
282 than CTR30 (Figure 3D), suggesting a developmental upregulation of the *Htr3a* gene during the P10-P30
283 period. Similarly, L4 VIP^+ cells expressed increasing quantities of *Htr3a* mRNA between CTR10, CTR15, and
284 CTR30 (Figure 3E). L1 VIP^+ cells increased in expression between CTR10 and CTR15, but not significantly
285 between CTR15 and CTR30.

286 In the ontogenetic model for $NDNF^+$ cell development (Table 1B), there was also a significant
287 interaction between condition and layer, though with smaller contrasts, likely related to the lower
288 number of puncta labeled in this population. There was a significant difference in *Htr3a* levels of L1 $NDNF^+$
289 cells between CTR30 and CTR10, but not between CTR15 and other ages (Figure 3C). Number of puncta
290 also increased between P10 and P30 in L2/3 $NDNF^+$ cells, but not in L4, where this population is extremely
291 sparse.

292 To verify the robustness of these results, we calculated the average puncta per cell for VIP^+ and
293 $NDNF^+$ populations within layers for each animal then subjected the averages to Mann-Whitney U tests.
294 Under control conditions, we found that average *Htr3a* puncta per cell increases during the course of
295 normal development in VIP^+ cells (Figure 3G,H). In L2/3 VIP^+ cells, mRNA expression is significantly higher

in CTR15 (M=28.82) compared to CTR10 (M=11.14) (U=35, p=0.0043). This trend continued between CTR15 and CTR30 (M=39.89), but did not reach significance (U=27, p=0.1797). Similar increases were seen in L4 VIP$^+$ cells (Figure 3H). Average puncta per cell trended upward between CTR10 (M=6.56) and CTR15

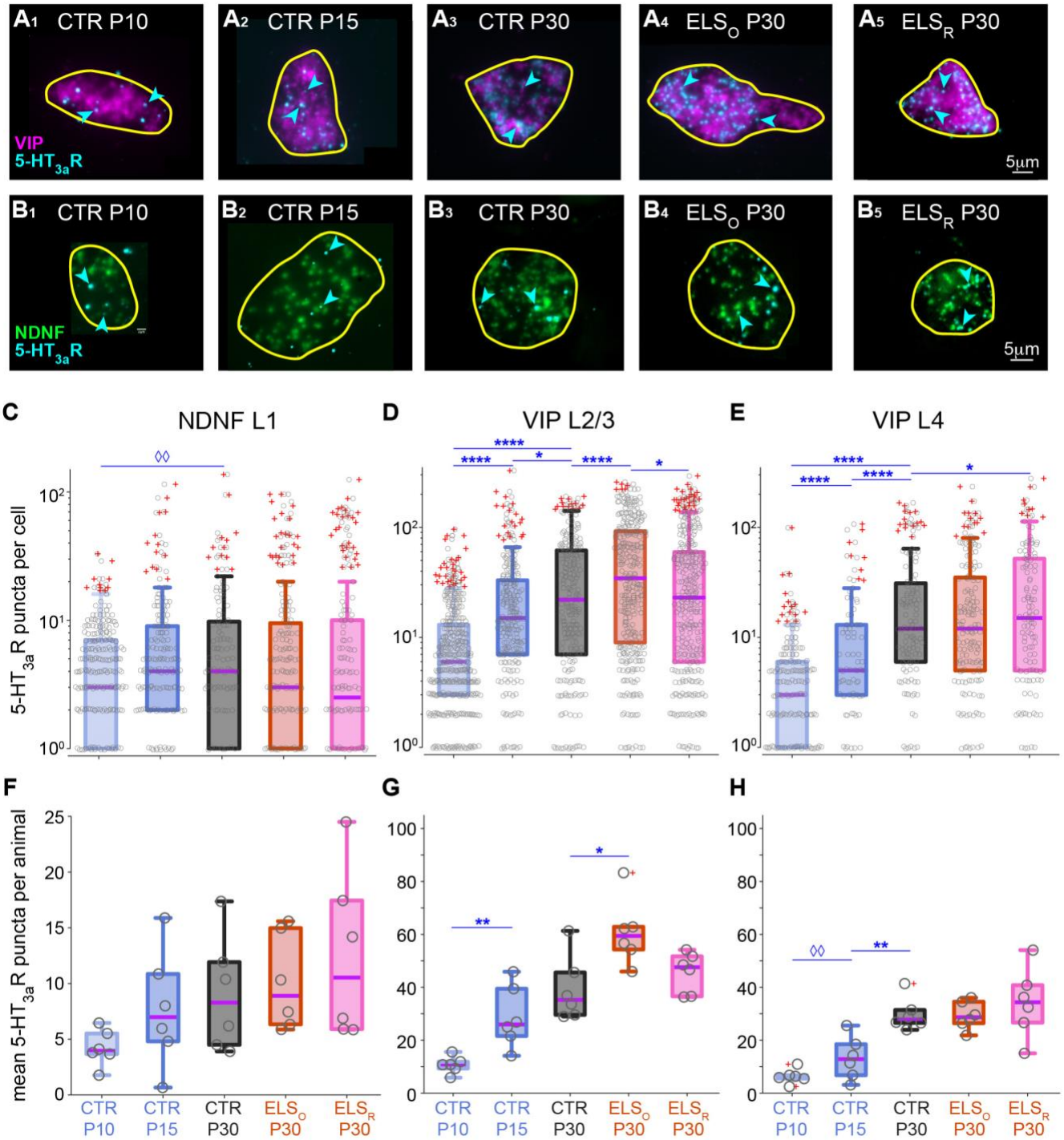

Figure 3: *Htr3a* mRNA increases during the P10-P30 period under control conditions for both cell populations, and is elevated in VIP+ cells by ELS, most prominently in L2/3. (A) L2/3 VIP (*pink*) and *Htr3a* mRNA puncta (*cyan*), in cells representing median expression of *Htr3a* within the highest quartile for each treatment group. (B) L1 NDNF (*green*) and *Htr3a* puncta (*cyan*), in cells representing median expression of *Htr3a* within the highest quartile for each treatment group. (C-E) Log-scale distributions of *Htr3a* puncta per cell within each group. Significant results from the GLMMs are marked above. (F-H) Comparisons of average expression profiles by animal; significant results from Mann Whitney U tests are marked above. ***p <0.002, **p <0.01, *p <0.05, ◊◊p <0.08. Arrowheads indicate a subset of *Htr3a* mRNA puncta.

299 (M=13.48) (*U*=29, *p*=0.09307), then increased significantly between CTR15 and CTR30 (M=28.80) (*U*=34,
300 *p*=0.0087). No significant group differences were found between control groups for L1 VIP$^+$ cells.

301 For NDNF$^+$ cells, though there is a trend toward increasing average expression, we did not find any
302 significant group differences (Figure 3F).

A. Ontogenetic Model of VIP Cell *Htr3a* mRNA Expression					
	χ2 (df), *P*		L1 Contrast +/- SE (z ratio, *P*)	L2/3 Contrast +/- SE (z ratio, *P*)	L4 Contrast +/- SE (z ratio, *P*)
Condition	95.90 (2), ***< 2.2e-16***	**Ctr10 vs Ctr15**	-2.010 ± 0.236 (-8.519, ***<0.0001***)	-0.895 ± 0.159 (-5.622, ***<0.001***)	-0.738 ± 0.164 (-4.495, ***<0.0001***)
Layer	276.64 (2), ***< 2.2e-16***	**Ctr10 vs Ctr30**	-2.233 ± 0.235 (-9.516, ***<0.0001***)	-1.29 ± 0.159 (-8.114, ***<0.0001***)	-1.45 ± 0.162 (-8.945, ***<0.0001***)
Cond x Layer	108.65 (4), ***< 2.2e-16***	**Ctr15 vs Ctr30**	-0.223 ± 0.173 (-1.288, *0.1976*)	-0.395 ± 0.159 (-2.489, ***0.0128***)	-0.712 ± 0.162 (-4.391, ***<0.0001***)
B. Ontogenetic Model of NDNF Cell *Htr3a* mRNA Expression					
	χ2 (df), *P*		L1 Contrast +/- SE (z ratio, *P*)	L2/3 Contrast +/- SE (z ratio, *P*)	L4 Contrast +/- SE (z ratio, *P*)
Condition	7.12 (2), ***0.02844***	**Ctr10 vs Ctr15**	-0.461 ± 0.291 (-1.581, *0.1707*)	0.417 ± 0.315 (1.325, *0.1851*)	0.58 ± 0.316 (1.838, *0.198*)
Layer	21.40 (2), ***2.258e-05***	**Ctr10 vs Ctr30**	-0.759 ± 0.289 (-2.624, ***0.0261***)	-1.126 ± 0.311 (-3.617, ***0.0004***)	0.464 ± 0.375 (1.238, *0.3234*)
Cond x Layer	198.53 (4), ***< 2.2e-16***	**Ctr15 vs Ctr30**	-0.298 ± 0.308 (-0.968, *0.3332*)	-1.543 ± 0.322 (-4.800, ***<0.0001***)	-0.116 ± 0.392 (-0.296, *0.7669*)
C. ELS Model of VIP Cell *Htr3a* mRNA Expression					
	χ2 (df), *P*		L1 Contrast +/- SE (z ratio, *P*)	L2/3 Contrast +/- SE (z ratio, *P*)	L4 Contrast +/- SE (z ratio, *P*)
Condition	14.11 (2), ***0.0009***	**Ctr30 vs RELS**	-0.3919 ± 0.115 (-3.415, ***0.0019***)	-0.1248 ± 0.102 (-1.229, *0.2193*)	-0.2604 ± 0.104 (-2.510, ***0.0362***)
Layer	410.45 (2), ***< 2.2e-16***	**Ctr 30 vs OELS**	-0.3677 ± 0.115 (-3.201, ***0.0021***)	-0.4126 ± 0.102 (-4.064, ***0.0001***)	-0.0822 ± 0.104 (-0.792, *0.4283*)
Cond x Layer	395.49 (4), ***< 2.2e-16***	**RELS vs OELS**	0.0242 ± 0.108 (0.223, *0.8232*)	-0.2878 ± 0.101 (-2.840, ***0.0068***)	0.1782 ± 0.103 (1.727, *0.1263*)
D. ELS Model of NDNF Cell *Htr3a* mRNA Expression					
	χ2 (df), *P*		L1 Contrast +/- SE (z ratio, *P*)	L2/3 Contrast +/- SE (z ratio, *P*)	L4 Contrast +/- SE (z ratio, *P*)
Condition	1.50 (2), *0.4718*	**Ctr30 vs RELS**	-0.2956 ± 0.26 (-1.135, *0.5008*)	0.1966 ± 0.269 (0.732, *0.4642*)	0.8418 ± 0.376 (2.240, *0.0743*)
Layer	81.37 (2), ***<2e-16***	**Ctr 30 vs OELS**	-0.0449 ± 0.26 (-0.172, *0.8632*)	0.8448 ± 0.27 (3.127, ***0.0053***)	0.2193 ± 0.357 (0.614, *0.5393*)
Cond x Layer	126.11 (4), ***<2e-16***	**RELS vs OELS**	0.2507 ± 0.259 (0.966, *0.5008*)	0.6482 ± 0.265 (2.451, ***0.0214***)	-0.6225 ± 0.317 (-1.964, *0.0743*)

Table 1: Summary of each of the four generalized linear mixed models (GLMMs) assessing differences in Htr3a mRNA expression. Contrasts were performed on estimated marginal means resulting from the models, with values reported on a log scale. Significant p values with Benjamini-Hochberg adjustment are in **bold.**

303 *ELS Increases 5HT3a mRNA Expression in VIP$^+$ Cells in a Layer-Specific Manner*

304 Similar to the ontogenetic models, our ELS model of VIP$^+$ cells revealed a significant interaction
305 between condition and layer, with contrasts showing distinct layer-specific effects of each stress group
306 (Table 1C). In the L2/3 VIP$^+$ population, *Htr3a* was significantly higher in ELS$_O$ compared to CTR30, whereas
307 there was no significant contrast between ELS$_R$ and CTR30 (Figure 3D). Conversely, among L4 VIP$^+$ cells,
308 mRNA expression in ELS$_R$ was higher than CTR30, with no significant difference between ELS$_O$ and CTR30
309 (Figure 3E). Both ELS$_O$ and ELS$_R$ contained significantly more *Htr3a* puncta in L1 compared to CTR30,
310 though these cells are few.

311 The ELS model of NDNF$^+$ cells identified a significant interaction between layer and condition but did
312 not identify condition on its own as a significant predictor of *Htr3a* puncta levels, diverging from the
313 other models (Table 1D). No differences were found in L1 NDNF$^+$ cells. Indeed, the only significant
314 contrast found was between ELS$_O$ and ELS$_R$ L2/3 NDNF$^+$ cells, sparse populations containing only 64 and
315 51 cells, respectively.

316 Comparing averages between animals, we found that *Htr3a* mRNA expression in L2/3 VIP$^+$ cells is
317 greater in ELS$_O$ (60.86, n=6) compared to CTR30 (M=39.89) (U=33, p=0.0152), while ELS$_R$ (M=45.65) did
318 not differ significantly from controls (U=26, p=0.2403) (Figure 3G). Mann-Whitney U tests did not reveal
319 any significant differences between ELS$_R$ or ELS$_O$ with controls in L1 or L4 VIP$^+$ cells. No significant group
320 differences were found between stress groups and controls for NDNF$^+$ cells in any layers.

321 *NDNF mRNA Expression Decreases During Normal Development*

322 To evaluate whether development or stress affected levels of NDNF mRNA within NDNF$^+$ cells, we
323 quantified *NDNF* in all NDNF cells across layers 1 through 4. Similar to our approach with *Htr3a* data, we
324 examined *NDNF* expression pooled within each treatment condition using two separate GLM models for
325 normal development and for evaluation of ELS effects. In our ontogenetic model of NDNF$^+$ cell
326 development, there was a significant interaction between condition and layer, such that the variance in
327 number of *NDNF* puncta according to condition depended on layer (Table 2A). Post-hoc tests examining
328 differences between conditions within layers found that L1 cells expressed significantly more puncta in
329 Ctr10 than Ctr30 (Figure 4B), suggesting a developmental downregulation of *NDNF* expression during this
330 window. This trend was also noted between Ctr10 vs Ctr 15 animals, as well as Ctr15 vs Ctr30 animals, but
331 did not reach significance in these individual contrast analyses. No developmental differences were seen
332 in L2/3 NDNF$^+$ cells. L4 contrasts yielded mixed results: a non-significant decline in expression was
333 observed between Ctr10 to Ctr15, accompanied by an unexpected significant increase in expression
334 between Ctr15 to Ctr30. As there were relatively few NDNF$^+$ cells in L4 compared to L1, and no previous
335 description of L4 NDNF$^+$ neurons in the existing literature to our awareness, we interpret these findings
336 cautiously.

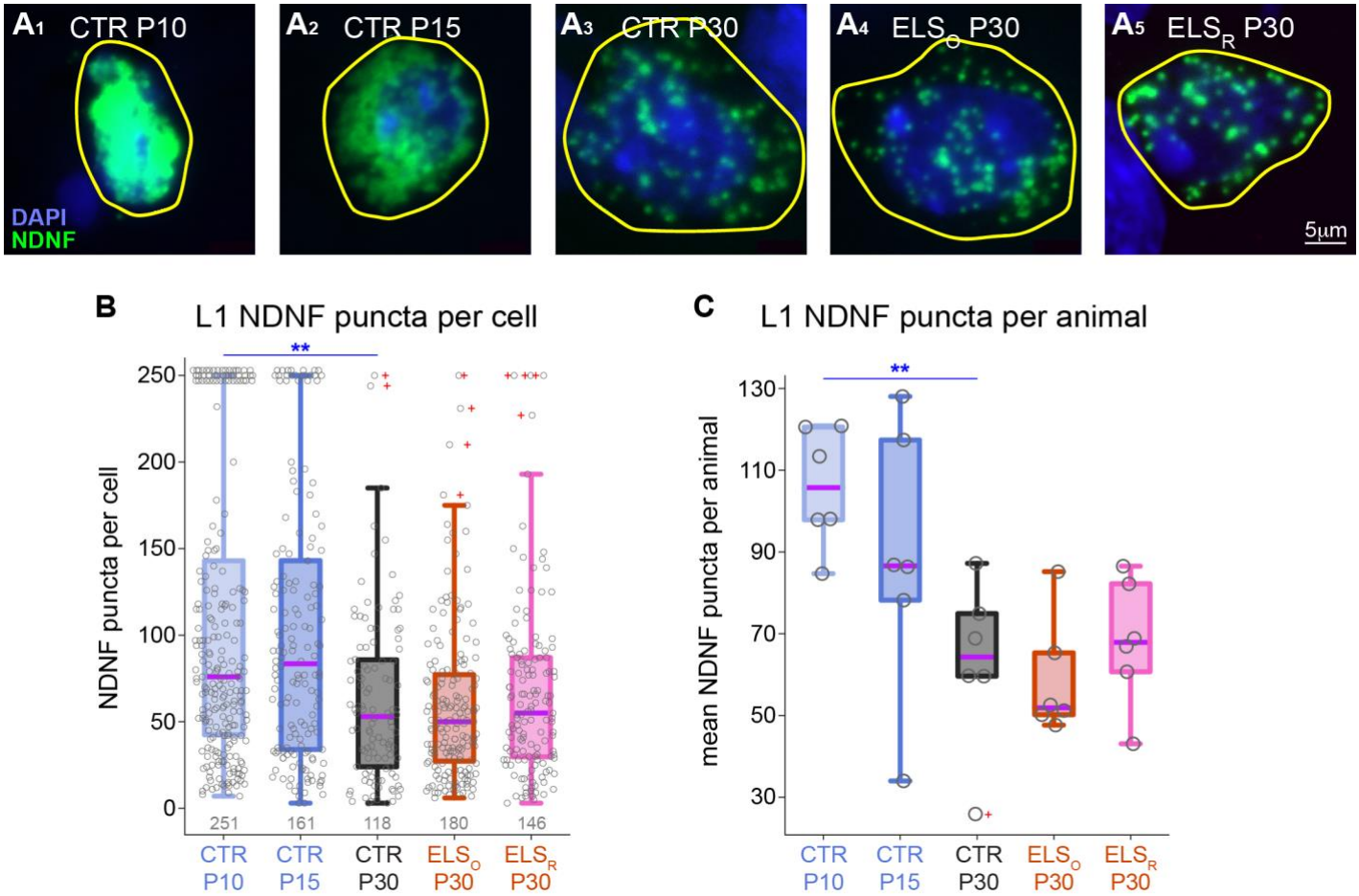

Figure 4: Layer 1 NDNF neurons show a developmental decrease of *NDNF* mRNA. (A) L1 *NDNF* mRNA puncta (*green*), in cells representing median expression of *NDNF* within the highest quartile for each treatment group. (B) Distributions of L1 *NDNF* puncta per cell within each group. Significant results from the GLMMs are marked above. Grey numbers indicate number of cells per treatment group. Grey circles in boxplots show individual cell data. (C) Within L1 NDNF cells, comparisons of average *NDNF* expression profiles by animal; significant results from Mann Whitney U tests are marked above. Grey circles in boxplots show individual animal data. ****p <0.001, ***p <0.002, **p <0.01, *p <0.05, ◊◊p <0.08, ◊p <0.14.

In line with our treatment of *Htr3a* data, we calculated the mean *NDNF* puncta per cell within L1 for each animal and subjected these averages to Mann-Whitney U tests. Under control conditions, we again observed a decline in *NDNF* expression during normal development (Figure 4C). mRNA expression was significantly greater in Ctr10 (M=105.9) compared to Ctr30 (M=62.71) (U=35, p=0.004329). There was a consistent downward trend from Ctr10 to Ctr15, and between Ctr15 to Ctr30, though these individual comparisons did not reach significance, consistent with the outcome of our GLMM. No significant differences were found within L2/3 or L4 under normal development.

NDNF mRNA Expression is Mostly Unaffected by ELS

The ELS model of NDNF$^+$ cells identified a significant interaction between layer and condition but did not identify condition on its own as a significant predictor of NDNF puncta levels (Table 2B). No significant contrasts were found between conditions for L1 (Figure 4B) or L2/3 NDNF$^+$ cells. In L4, NDNF expression was significantly greater in RELS animals compared to P30 controls, whereas expression was

349 significantly lower in OELS animals compared to P30 controls. The largest difference was observed
350 between the stress conditions themselves, with significantly greater L4 expression levels in RELS
351 compared to OELS.

352 Comparing averages between animals, no significant effects of stress emerged in either L1 (Figure 4C)
353 or L2/3. In L4, similar to our GLMM analyses, RELS animals (M=92.5) showed greater expression
354 compared to Ctr30 (M=40.5) (U=15, p=0.036) and to OELS (M=36.3) (U=29, p=0.0087). There was no
355 difference found between OELS vs. Ctr30 subjects. Again, because of the low number of cells sampled
356 within this population, and with some animals lacking L4 NDNF data altogether, these findings should be
357 interpreted with caution as they may be spurious due to insufficient sampling.

Ontogenetic Model of *NDNF* mRNA Expression					
	χ2(df), *P*		**L1 Contrast +/- SE (z ratio, *P*)**	**L2/3 Contrast +/- SE (z ratio, *P*)**	**L4 Contrast +/- SE (z ratio, *P*)**
Condition	9.6061 (2), ***0.008205***	**Ctr10 - Ctr15**	0.2381 ± 0.184 (1.291, *0.1968*)	-0.2257 ± 0.19 (-1.186, *0.3535*)	0.3223 ± 0.191 1.69, *0.1366*)
Layer	1167.3571 (2), ***< 2.2e-16***	**Ctr10 - Ctr30**	0.5718 ± 0.185 (3.099, ***0.0058***)	-0.2598 ± 0.193 (-1.347, *0.3535*)	-0.1901 ± 0.195 (-0.975, *0.3298*)
Cond x Layer	351.3672 (4), ***<2.2e-16***	**Ctr15 - Ctr30**	0.3337 ± 0.197 (1.692, *0.136*)	-0.0341 ± 0.202 (-0.169, *0.8659*)	-0.5123 ± 0.206 (-2.482, ***0.0392***)
ELS Model of *NDNF* mRNA Expression					
	χ2(df), *P*		**L1 Contrast +/- SE (z ratio, *P*)**	**L2/3 Contrast +/- SE (z ratio, *P*)**	**L4 Contrast +/- SE (z ratio, *P*)**
Condition	1.0487 (2), *0.5919*	**Ctr30 vs RELS**	-0.1102 ± 0.144 (-0.766, *0.6656*)	-0.2801 ± 0.15 (-1.872, *0.0919*)	-0.5842 ± 0.155 (-3.78, ***0.0002***)
Layer	47.4234 (2), ***<5.037e-11***	**Ctr 30 vs OELS**	0.0293 ± 0.144 (0.204, *0.8384*)	0.0658 ± 0.15 (0.44, *0.6597*)	0.3502 ± 0.155 (2.255, ***0.0241***)
Cond x Layer	387.08825 (4), ***<2.2e-16***	**RELS vs OELS**	0.1395 ± 0.144 (0.971, *0.6656*)	0.346 ± 0.146 (2.376, *0.0526*)	0.9344 ± 0.148 (6.314, ***<0.0001***)

Table 1: Summary of the two GLMMs assessing differences in NFNF mRNA expression. Contrasts were performed on estimated marginal means resulting from the models, with values reported on a log scale. Significant p values with Benjamini-Hochberg adjustment are in **bold**.

358 ## DISCUSSION

359 5-HT3R expressing inhibitory interneurons, particularly L1 NDNF$^+$ and L2/3 VIP$^+$ cells, have gained
360 increased attention in recent years as important regulators of cortical circuitry. These superficial neurons
361 influence developmental plasticity and integrate top-down and bottom-up information to gate response
362 properties of other cortical neurons (Takesian et al., 2018; Pardi et al., 2023). The gene encoding the 3A
363 protein subunit, *Htr3a,* present in all functional 5-HT3Rs (Boyd et al., 2002), has been identified as a
364 genetic locus that is susceptible to ELS and may be linked to clinical outcomes in neuropsychiatric
365 conditions (Rajkumar and Mahesh, 2010; Gupta et al., 2016; Perroud et al., 2016). By examining the *in situ*
366 cell-specific expression of *Htr3a* across the ACx critical period, our data provide context for how ELS may

interact with this gene to produce functional aberrations in the circuits involving NDNF$^+$ and VIP$^+$ interneurons.

Developmentally we found that in ACx, VIP$^+$ and NDNF$^+$ cell densities decreased dramatically between P10 and P30 in control animals, with much of the reduction in cell density occurring by P15, midway through the ACx critical period and following ear opening at ~P11 (Figure 2). For both cell types, CTR10 animals showed substantial variation in cell density that largely collapsed by P15, indicating that at this time point we sampled a rapid shift in the development of the cell populations. The timing of this decrease following the increased sensory input of ear opening is suggestive of an activity-dependent process and may reflect apoptosis. Developmental apoptosis has not been described in auditory cortex, but in the auditory brainstem, hearing onset precedes a period of cell death (Tierney and Moore, 1997), and apoptosis across cortical regions is regulated based on activity levels (Blanquie et al., 2017). Previous work has established that interneurons derived from the caudal ganglionic eminence (CGE), which constitute the bulk of 5-HT3R cells, undergo programmed cell death, and that this occurs in an activity-dependent manner that relies on calcineurin signaling during specific periods in postnatal development (De Marco Garcia et al., 2011; Priya et al., 2018). VIP interneurons have been singled out as an exception to this rule, with some experiments suggesting that they are exempt from this activity-dependent effect. However, more recent work discovered that different mechanisms govern the survival of distinct 5-HT3R subpopulations, with VIP interneuron fate specifically tied to serotonergic input during active periods of programmed cell death (Wong et al., 2022). The ontogeny of serotonin metabolism in ACx is consistent with this result, increasing between P10 and P15 in rats (Basura et al., 2008), and the 5-HT3Rs present in these cells are excitatory. Thus the sharp decline in densities of both of these inhibitory cell types may reflect cell death that is cued by the increased activity accompanying ear opening.

Our data show that ELS attenuates the developmental decline in both NDNF$^+$ and VIP$^+$ cell density in a layer-specific manner (Figure 2). In ELS animals, we found increased cell density in L2/3 VIP$^+$ cells at P30 compared to controls. In ELS$_O$ animals, these cells also expressed higher levels of *Htr3a* (Figure 3), raising the possibility that ELS may impact VIP$^+$ cell survival through upregulation of the 5-HT3A gene, a possibility consistent with a known protective role of 5-HT in cell survival (Vitalis and Parnavelas, 2003; Barzegar-Fallah et al., 2023), though that action may be context dependent (Ju Yeon and Yeon Hee, 2005; Aminzadeh, 2017). Similar effects were seen in prefrontal cortex, where ELS in rats increased the density of VIP cells (Pascual et al., 2006). Further work is needed to confirm the specific contributions of 5-HT3A, given the milieu of changes brought about by ELS on the serotonin system (Lages et al., 2021; Lipsky et al., 2022). Similarly, L1 NDNF$^+$ cell density was also significantly increased by stress, with P30 ELS$_R$ animals maintaining cell populations on par with P15 controls. These cells, however, did not show a marked increase in *Htr3a* expression. It is possible that other changes, such as glutamatergic inputs known to influence interneuron cell survival, may instead influence NDNF cell fate under these conditions (Wong et al., 2022).

The results of our GLMM analyses revealed that *Htr3a* mRNA was developmentally upregulated in VIP$^+$ cells in all layers that were examined (L1, L2/3, and L4), whereas levels remained relatively stable in

405 NDNF$^+$ cells (Figure 3; Table 1). Note that *Htr3a* expression was ~four-fold higher in VIP$^+$ than NDNF$^+$ cells,
406 consistent with a stronger depolarizing effect of serotonin on VIP$^+$ cells mediated at least in part by 5-
407 HT3Rs (Poorthuis et al., 2018; Pronneke et al., 2020; Wong et al., 2022). Stress induction increased *Htr3a*
408 expression beyond control levels in VIP$^+$ cells, with ELS$_O$ animals showing substantial increases in L2/3,
409 and ELS$_R$ animals showing increased levels in L4. While it is unclear why the two stress induction methods
410 used here would not cause equivalent changes, it is well established that ELS effects can vary based on
411 many parameters including type of stressor, animal age at induction, duration and unpredictability of
412 stress, and individual genetic susceptibility (Lehmann and Feldon, 2000; Rincon-Cortes and Sullivan,
413 2014). Neither form of ELS had a substantial impact on *Htr3a* expression in NDNF$^+$ cells. These findings
414 were largely recapitulated when using single animal as the unit of analysis. Though the extent to which
415 elevated *Htr3a* mRNA translates to increased protein production is unknown, differentially expressed
416 genes generally show greater correlations between mRNA and protein quantity compared to genes that
417 maintain stable expression profiles (Koussounadis et al., 2015). Increased *Htr3a* is consistent with several
418 studies in which developmental stress altered 5-HT3R expression in cortical regions, though these
419 approaches did not evaluate cell-type specificity (Perroud et al., 2016; Moradi-Kor et al., 2020; Zolfaghari
420 et al., 2021).

421 Increased expression of functional excitatory 5-HT3Rs over development and by early-life stress,
422 combined with increased NDNF$^+$ and VIP$^+$ numbers, could alter both cortical plasticity and auditory
423 processing and contribute to the temporal processing deficits that follow ELS. Both VIP$^+$ and NDNF$^+$
424 interneurons integrate inputs from primary auditory thalamus and neuromodulatory regions
425 (Kuchibhotla et al., 2017; Poorthuis et al., 2018; Vattino et al., 2025), responding with high selectivity to
426 relevant or novel features of complex auditory stimuli (Zhu et al., 2015; Cohen-Kashi Malina et al., 2021;
427 Rikhye et al., 2021; Yarden et al., 2022; Jamali et al., 2024; Sweeney et al., 2025), particularly in specific
428 behavioral contexts (Ding et al., 2025; Sweeney et al., 2025). The involvement of these neurons in
429 context-dependent responses to temporally-varying behaviorally relevant sounds may be disrupted by
430 ELS-induced circuit changes. Inhibitory fibers from VIP$^+$ cells target a combination of intracolumnar cell
431 bodies of PV and somatostatin (SST) interneurons (Figure 1a), forming disinhibitory circuits that increase
432 pyramidal cell activity (David et al., 2007; Hioki et al., 2013; Pi et al., 2013; Zhang et al., 2022). Increased
433 expression of the excitatory 5-HT3R along with increased numbers of VIP$^+$ cells could thus enhance
434 pyramidal excitability, though this may be counteracted by circuit effects involving SST interneurons
435 (Batista-Brito et al., 2017; Ferguson et al., 2023). NDNF$^+$ cells, though fewer in number than VIP$^+$, are
436 regularly spaced throughout L1 and exert a powerful influence over cortical dynamics, integrating top-
437 down signals with bottom-up sensory input to gain-modulate cortical columns (Cohen-Kashi Malina et al.,
438 2021; Vattino et al., 2025). They receive inputs from widespread sources whose fibers course through L1,
439 and through volume transmission coordinate a mixture of postsynaptic targets that include PV cells, VIP$^+$
440 cells, and pyramidal cell apical dendrites to affect state-dependent sensory processing (Letzkus et al.,
441 2011; Overstreet-Wadiche and McBain, 2015; Hartung et al., 2024; Sweeney et al., 2025). Both cell types
442 have been implicated in plasticity (Takesian et al., 2018; Melzer et al., 2021; Williams et al., 2025).
443 Developmentally, shifts in NDNF$^+$ and VIP$^+$ activity during the ACx critical period may dramatically alter

444 circuit dynamics. Indeed, developmental perturbation of NDNF$^+$ or VIP$^+$ activity produced perceptual
445 deficits along with altered cortical map organization and response properties of pyramidal cells, including
446 sensory-evoked firing, phase-locking, and response selectivity (Batista-Brito et al., 2017; Che et al., 2018;
447 Takesian et al., 2018), indicating a role for these cells in developmental plasticity. Thus alterations to
448 NDNF$^+$ and VIP$^+$ dynamics by stress, via a combined action of increased sensitivity to serotonin and
449 increased cell survival, could lead to imbalanced excitation within affected cortical columns, impairing
450 perception and learning.

451 Because both VIP$^+$ and NDNF$^+$ cells target PV interneurons (Pi et al., 2013; Hartung et al., 2024), PV
452 cells may be affected by changes to 5-HT3R interneurons. PV neurons contribute to accurate temporal
453 processing and drive critical period plasticity (Krause et al., 2019; Reh et al., 2020; Nocon et al., 2023),
454 both of which are shifted by ELS (Pattwell and Bath, 2017; Ye et al., 2023; An et al., 2025; Mazi et al., 2025;
455 Rosen and Huyck, 2025). ELS is known to affect PV cells, decreasing PV expression and reducing cell
456 density in ACx and other regions (Goodwill et al., 2018; Sunthimer et al., 2023; An et al., 2025; Mazi et al.,
457 2025). Further, cell survival in interneurons derived from the medial ganglionic eminence (MGE), including
458 PV cells, is affected by levels of cell activity (Denaxa et al., 2018). Thus PV survival may be reduced by
459 increased inhibitory tone from elevated NDNF$^+$ and VIP$^+$ cell populations containing more excitatory 5-
460 HT3Rs, leading to disruption of inhibitory-excitatory dynamics. It is worth noting that because the
461 expression of PV is activity dependent, reduced PV cell density indicated by antibody binding assays may
462 in part reflect lowered activity in PV neurons. During development, reduced PV associates with delayed
463 critical period plasticity (Koh and Sng, 2016; Reh et al., 2020), and auditory temporal processing deficits
464 can be rescued by PV activation (Masri et al., 2021; Masri et al., 2024). PV activity enables accurate
465 responses to temporally-varying stimuli (Nocon et al., 2023); for example PV cells respond more strongly
466 to short gaps than pyramidal cells (Keller et al., 2018). Thus PV reduction by ELS could contribute to the
467 ELS-induced temporal processing deficits that have been recently described in gerbils, rats, and mice (Ye
468 et al., 2023; An et al., 2025; Mazi et al., 2025).

469 Finally, we examined expression of *NDNF* mRNA within NDNF$^+$ cells to reveal a developmental decline
470 in *NDNF* that was not affected by ELS. NDNF is a secretory protein that promotes cell survival, migration
471 and neurite outgrowth, while protecting against excitotoxity and downregulating apoptosis-related
472 pathways (Kuang et al., 2010; Cheng et al., 2023a; Liu et al., 2024). While it is not established whether
473 NDNF$^+$ L1 neurons have a secretory role, their propensity for volume transmission suggests that these
474 cells could provide broad trophic support to their targets (Olah et al., 2009). The large drop in *NDNF*
475 mRNA from P10 to P30 coincides with ACx critical period plasticity and increased activity following ear
476 opening, a period when cortical circuitry is refined based on activity levels and trophic support from
477 neural growth factors (Catapano et al., 2001). At P10 we identified many cells containing a very high
478 density of NDNF puncta (Figure 4B); this declined over development and rarely occurred by P30.
479 Although this study did not evaluate the role of NDNF as a trophic factor, the gradual decline of NDNF
480 coincides with reduced NDNF$^+$ and VIP$^+$ cell density. However, NDNF mRNA levels remained stable with
481 ELS, despite increased numbers of NDNF$^+$ and VIP$^+$ cells. Thus NDNF may not contribute to the increased

482 NDNF$^+$ and VIP$^+$ cell densities seen with ELS. It is possible that other trophic factors and/or increased
483 activity levels in ELS cells, predicted by increased 5HT3aRs, contributes to the higher number of cells
484 following ELS.

485 The present study identified changes to 5-HT3R cell populations as a function of development and
486 early-life stress, including an increase in cell density and *Htr3a* expression following ELS. The functional
487 implications of these differential expression profiles will need to be evaluated by assessing the
488 responsiveness of these subpopulations to serotonergic input and measuring the behavior of their
489 synaptic targets. Future studies are needed to reveal the full range of functional sequelae resulting from
490 these effects and shed further light on potential interventions to mitigate such maladaptive alterations
491 during development.

492 **REFERENCES**

493 Adler LE, Cawthra EM, Donovan KA, Harris JG, Nagamoto HT, Olincy A, Waldo MC (2005) Improved p50 auditory
494 gating with ondansetron in medicated schizophrenia patients. Am J Psychiatry 162:386-388.

495 Aminzadeh A (2017) Protective effect of tropisetron on high glucose induced apoptosis and oxidative stress in PC12
496 cells: roles of JNK, P38 MAPKs, and mitochondria pathway. Metab Brain Dis 32:819-826.

497 An P, Fang Y, Cheng Y, Liu H, Yang W, Shan Y, de Villers-Sidani E, Zhang G, Zhou X (2025) Acoustic enrichment
498 prevents early life stress-induced disruptions in sound azimuth processing. J Neurosci 45.

499 Baram TZ, Davis EP, Obenaus A, Sandman CA, Small SL, Solodkin A, Stern H (2012) Fragmentation and
500 unpredictability of early-life experience in mental disorders. Am J Psychiatry 169:907-915.

501 Barzegar-Fallah A, Alimoradi H, Dunlop JL, Torbati E, Baird SK (2023) Serotonin type-3 receptor antagonists
502 selectively kill melanoma cells through classical apoptosis, microtubule depolymerisation, ERK activation,
503 and NF-kappaB downregulation. Cell Biol Toxicol 39:1119-1135.

504 Basura GJ, Abbas AI, O'Donohue H, Lauder JM, Roth BL, Walker PD, Manis PB (2008) Ontogeny of serotonin and
505 serotonin2A receptors in rat auditory cortex. Hear Res 244:45-50.

506 Bates D, Mächler M, Bolker B, Walker S (2015) Fitting Linear Mixed-Effects Models Using lme4. Journal of Statistical
507 Software 67:1-48.

508 Bath KG, Schilit A, Lee FS (2013) Stress effects on BDNF expression: effects of age, sex, and form of stress.
509 Neuroscience 239:149-156.

510 Batista-Brito R, Vinck M, Ferguson KA, Chang JT, Laubender D, Lur G, Mossner JM, Hernandez VG, Ramakrishnan C,
511 Deisseroth K, Higley MJ, Cardin JA (2017) Developmental Dysfunction of VIP Interneurons Impairs Cortical
512 Circuits. Neuron 95:884-895 e889.

513 Blanquie O, Yang JW, Kilb W, Sharopov S, Sinning A, Luhmann HJ (2017) Electrical activity controls area-specific
514 expression of neuronal apoptosis in the mouse developing cerebral cortex. Elife 6.

515 Boyd GW, Low P, Dunlop JI, Robertson LA, Vardy A, Lambert JJ, Peters JA, Connolly CN (2002) Assembly and cell
516 surface expression of homomeric and heteromeric 5-HT3 receptors: the role of oligomerization and
517 chaperone proteins. Mol Cell Neurosci 21:38-50.

518 Bravo JA, Dinan TG, Cryan JF (2014) Early-life stress induces persistent alterations in 5-HT1A receptor and serotonin
519 transporter mRNA expression in the adult rat brain. Front Mol Neurosci 7:24.

520 Campbell MJ, Lewis DA, Foote SL, Morrison JH (1987) Distribution of choline acetyltransferase-, serotonin-,
521 dopamine-beta-hydroxylase-, tyrosine hydroxylase-immunoreactive fibers in monkey primary auditory
522 cortex. J Comp Neurol 261:209-220.

523 Cases O, Vitalis T, Seif I, De Maeyer E, Sotelo C, Gaspar P (1996) Lack of barrels in the somatosensory cortex of
524 monoamine oxidase A-deficient mice: role of a serotonin excess during the critical period. Neuron 16:297-
525 307.

526 Castillo-Gomez E, Perez-Rando M, Belles M, Gilabert-Juan J, Llorens JV, Carceller H, Bueno-Fernandez C, Garcia-
527 Mompo C, Ripoll-Martinez B, Curto Y, Sebastia-Ortega N, Molto MD, Sanjuan J, Nacher J (2017) Early Social
528 Isolation Stress and Perinatal NMDA Receptor Antagonist Treatment Induce Changes in the Structure and
529 Neurochemistry of Inhibitory Neurons of the Adult Amygdala and Prefrontal Cortex. eNeuro 4.

530 Catapano LA, Arnold MW, Perez FA, Macklis JD (2001) Specific neurotrophic factors support the survival of cortical
531 projection neurons at distinct stages of development. J Neurosci 21:8863-8872.

532 Che A, Babij R, Iannone AF, Fetcho RN, Ferrer M, Liston C, Fishell G, De Marco Garcia NV (2018) Layer I Interneurons
533 Sharpen Sensory Maps during Neonatal Development. Neuron 99:98-116 e117.

534 Chen Y, Baram TZ (2016) Toward Understanding How Early-Life Stress Reprograms Cognitive and Emotional Brain
535 Networks. Neuropsychopharmacology 41:197-206.

536 Cheng W, Huang J, Fu XQ, Tian WY, Zeng PM, Li Y, Luo ZG (2023a) Intrathecal delivery of AAV-NDNF ameliorates
537 disease progression of ALS mice. Mol Ther 31:3277-3289.

538 Cheng Y, Chen R, Su B, Zhang G, Sun Y, An P, Fang Y, Zhang Y, Shan Y, de Villers-Sidani E, Wang Y, Zhou X (2023b)
539 Pairing with Enriched Sound Exposure Restores Auditory Processing Degraded by an Antidepressant. J
540 Neurosci 43:2850-2859.

541 Clement HW, Kirsch M, Hasse C, Opper C, Gemsa D, Wesemann W (1998) Effect of repeated immobilization on
542 serotonin metabolism in different rat brain areas and on serum corticosterone. J Neural Transm (Vienna)
543 105:1155-1170.

544 Cohen-Kashi Malina K, Tsivourakis E, Kushinsky D, Apelblat D, Shtiglitz S, Zohar E, Sokoletsky M, Tasaka GI, Mizrahi
545 A, Lampl I, Spiegel I (2021) NDNF interneurons in layer 1 gain-modulate whole cortical columns according to
546 an animal's behavioral state. Neuron 109:2150-2164 e2155.

547 David C, Schleicher A, Zuschratter W, Staiger JF (2007) The innervation of parvalbumin-containing interneurons by
548 VIP-immunopositive interneurons in the primary somatosensory cortex of the adult rat. Eur J Neurosci
549 25:2329-2340.

550 De Marco Garcia NV, Karayannis T, Fishell G (2011) Neuronal activity is required for the development of specific
551 cortical interneuron subtypes. Nature 472:351-355.

552 DeFelipe J, Hendry SH, Hashikawa T, Jones EG (1991) Synaptic relationships of serotonin-immunoreactive terminal
553 baskets on GABA neurons in the cat auditory cortex. Cereb Cortex 1:117-133.

554 Denaxa M, Neves G, Rabinowitz A, Kemlo S, Liodis P, Burrone J, Pachnis V (2018) Modulation of Apoptosis Controls
555 Inhibitory Interneuron Number in the Cortex. Cell Rep 22:1710-1721.

556 Ding X, Vogler NW, Tobin M, Garami L, Wood KC, Geffen MN (2025) The role of inhibitory neurons in novelty sound
557 detection in regular and random statistical contexts. bioRxiv.

558 Donato F, Rompani SB, Caroni P (2013) Parvalbumin-expressing basket-cell network plasticity induced by
559 experience regulates adult learning. Nature 504:272-276.

560 Dunn EC, Soare TW, Zhu Y, Simpkin AJ, Suderman MJ, Klengel T, Smith A, Ressler KJ, Relton CL (2019) Sensitive
561 Periods for the Effect of Childhood Adversity on DNA Methylation: Results From a Prospective,
562 Longitudinal Study. Biol Psychiatry 85:838-849.

563 Ferguson KA, Salameh J, Alba C, Selwyn H, Barnes C, Lohani S, Cardin JA (2023) VIP interneurons regulate cortical
564 size tuning and visual perception. Cell Rep 42:113088.

565 Gabard-Durnam LJ, McLaughlin KA (2019) Do Sensitive Periods Exist for Exposure to Adversity? Biological
566 Psychiatry 85:789-791.

567 Goodwill HL, Manzano-Nieves G, LaChance P, Teramoto S, Lin S, Lopez C, Stevenson RJ, Theyel BB, Moore CI,
568 Connors BW, Bath KG (2018) Early Life Stress Drives Sex-Selective Impairment in Reversal Learning by
569 Affecting Parvalbumin Interneurons in Orbitofrontal Cortex of Mice. Cell Rep 25:2299-2307 e2294.

570 Guadagno A, Belliveau C, Mechawar N, Walker CD (2021) Effects of Early Life Stress on the Developing Basolateral
571 Amygdala-Prefrontal Cortex Circuit: The Emerging Role of Local Inhibition and Perineuronal Nets. Front
572 Hum Neurosci 15:669120.

573 Gupta D, Prabhakar V, Radhakrishnan M (2016) 5HT3 receptors: Target for new antidepressant drugs. Neurosci
574 Biobehav Rev 64:311-325.
575 Hall IC, Rebec GV, Hurley LM (2010) Serotonin in the inferior colliculus fluctuates with behavioral state and
576 environmental stimuli. J Exp Biol 213:1009-1017.
577 Hartung J, Schroeder A, Perez Vazquez RA, Poorthuis RB, Letzkus JJ (2024) Layer 1 NDNF interneurons are
578 specialized top-down master regulators of cortical circuits. Cell Rep 43:114212.
579 Hioki H, Okamoto S, Konno M, Kameda H, Sohn J, Kuramoto E, Fujiyama F, Kaneko T (2013) Cell type-specific
580 inhibitory inputs to dendritic and somatic compartments of parvalbumin-expressing neocortical
581 interneuron. J Neurosci 33:544-555.
582 Horrocks M, Mohn JL, Jaramillo S (2025) The serotonergic psychedelic DOI impairs deviance detection in the
583 auditory cortex. J Neurophysiol 133:388-398.
584 Hurley LM, Pollak GD (2005) Serotonin modulates responses to species-specific vocalizations in the inferior
585 colliculus. J Comp Physiol A Neuroethol Sens Neural Behav Physiol 191:535-546.
586 Hurley LM, Hall IC (2011) Context-dependent modulation of auditory processing by serotonin. Hear Res 279:74-84.
587 Jamali S, Bagur S, Bremont E, Van Kerkoerle T, Dehaene S, Bathellier B (2024) Parallel mechanisms signal a
588 hierarchy of sequence structure violations in the auditory cortex. Elife 13.
589 Ju Yeon B, Yeon Hee S (2005) Blockade of 5-HT(3) receptor with MDL 72222 and Y 25130 reduces beta-amyloid
590 protein (25--35)-induced neurotoxicity in cultured rat cortical neurons. Eur J Pharmacol 520:12-21.
591 Kahne D, Tudorica A, Borella A, Shapiro L, Johnstone F, Huang W, Whitaker-Azmitia PM (2002) Behavioral and
592 magnetic resonance spectroscopic studies in the rat hyperserotonemic model of autism. Physiol Behav
593 75:403-410.
594 Keller CH, Kaylegian K, Wehr M (2018) Gap encoding by parvalbumin-expressing interneurons in auditory cortex. J
595 Neurophysiol 120:105-114.
596 Kessler RC et al. (2010) Childhood adversities and adult psychopathology in the WHO World Mental Health Surveys.
597 Br J Psychiatry 197:378-385.
598 Koh DX, Sng JC (2016) HDAC1 negatively regulates Bdnf and Pvalb required for parvalbumin interneuron
599 maturation in an experience-dependent manner. J Neurochem 139:369-380.
600 Koussounadis A, Langdon SP, Um IH, Harrison DJ, Smith VA (2015) Relationship between differentially expressed
601 mRNA and mRNA-protein correlations in a xenograft model system. Sci Rep 5:10775.
602 Koyama Y, Kondo M, Shimada S (2017) Building a 5-HT3A Receptor Expression Map in the Mouse Brain. Sci Rep
603 7:42884.
604 Kranz GS, Kasper S, Lanzenberger R (2010) Reward and the serotonergic system. Neuroscience 166:1023-1035.
605 Krause BM, Murphy CA, Uhlrich DJ, Banks MI (2019) PV+ Cells Enhance Temporal Population Codes but not
606 Stimulus-Related Timing in Auditory Cortex. Cereb Cortex 29:627-647.
607 Kuang XL, Zhao XM, Xu HF, Shi YY, Deng JB, Sun GT (2010) Spatio-temporal expression of a novel neuron-derived
608 neurotrophic factor (NDNF) in mouse brains during development. BMC Neurosci 11:137.
609 Kuchibhotla KV, Gill JV, Lindsay GW, Papadoyannis ES, Field RE, Sten TA, Miller KD, Froemke RC (2017) Parallel
610 processing by cortical inhibition enables context-dependent behavior. Nat Neurosci 20:62-71.
611 Kullander K, Topolnik L (2021) Cortical disinhibitory circuits: cell types, connectivity and function. Trends Neurosci
612 44:643-657.
613 Kuznetsova A, Brockhoff P, Christensen R (2017) lmerTest Package: Tests in Linear Mixed Effects Models. Journal
614 of Statistical Software 82:1-26.
615 Lages YVM, Rossi AD, Krahe TE, Landeira-Fernandez J (2021) Effect of chronic unpredictable mild stress on the
616 expression profile of serotonin receptors in rats and mice: a meta-analysis. Neurosci Biobehav Rev 124:78-
617 88.
618 Lee S, Hjerling-Leffler J, Zagha E, Fishell G, Rudy B (2010) The largest group of superficial neocortical GABAergic
619 interneurons expresses ionotropic serotonin receptors. J Neurosci 30:16796-16808.

620 Lehmann J, Feldon J (2000) Long-term biobehavioral effects of maternal separation in the rat: consistent or
621 confusing? Rev Neurosci 11:383-408.
622 Lenth R (2023) emmeans: Estimated Marginal Means, aka Least-Squares Means. In.
623 Letzkus JJ, Wolff SB, Meyer EM, Tovote P, Courtin J, Herry C, Luthi A (2011) A disinhibitory microcircuit for
624 associative fear learning in the auditory cortex. Nature 480:331-335.
625 Lipsky RK, McDonald CC, Souders MC, Carpio CC, Teitelman AM (2022) Adverse childhood experiences, the
626 serotonergic system, and depressive and anxiety disorders in adulthood: A systematic literature review.
627 Neurosci Biobehav Rev 134:104495.
628 Liu Y, Wang Z, Zhang X, Li S, Wu W, Li X, Yang Y (2020) A sex-dependent delayed maturation of visual plasticity
629 induced by adverse experiences in early childhood. Neurobiol Stress 13:100256.
630 Liu Y, Ren J, Bai R, He S, Peng Z, Yin W, Guo R, Niu J, Zhang W, Xia Z, Fan X, Yang K, Li B, Yang H, Song H, Xie J
631 (2024) Overexpression of NDNF Improves the Cytoprotective Effects of Aged Human Bone Marrow
632 Mesenchymal Stem Cells by Modulating Oxidative Stress and Apoptosis. Stem Cells Dev 33:432-437.
633 Malave L, van Dijk MT, Anacker C (2022) Early life adversity shapes neural circuit function during sensitive postnatal
634 developmental periods. Transl Psychiatry 12:306.
635 Masri S, Mowery TM, Fair R, Sanes DH (2024) Developmental hearing loss-induced perceptual deficits are rescued
636 by genetic restoration of cortical inhibition. Proc Natl Acad Sci U S A 121:e2311570121.
637 Masri S, Chan N, Marsh T, Zinsmaier A, Schaub D, Zhang L, Wang W, Bao S (2021) Chemogenetic Activation of
638 Cortical Parvalbumin-Positive Interneurons Reverses Noise-Induced Impairments in Gap Detection. J
639 Neurosci 41:8848-8857.
640 Mazi AR, Karakoc Y, Demirtas C, Aykin U, Yildirim M (2025) Extracellular Matrix Alterations Due to Early-Life
641 Adversity: Implications for Auditory Learning in Male Sprague-Dawley Rats. Mol Neurobiol 62:6490-6502.
642 Melzer S, Newmark ER, Mizuno GO, Hyun M, Philson AC, Quiroli E, Righetti B, Gregory MR, Huang KW, Levasseur J,
643 Tian L, Sabatini BL (2021) Bombesin-like peptide recruits disinhibitory cortical circuits and enhances fear
644 memories. Cell 184:5622-5634 e5625.
645 Moradi-Kor N, Dadkhah M, Ghanbari A, Rashidipour H, Bandegi AR, Barati M, Kokhaei P, Rashidy-Pour A (2020)
646 Protective Effects of Spirulina platensis, Voluntary Exercise and Environmental Interventions Against
647 Adolescent Stress-Induced Anxiety and Depressive-Like Symptoms, Oxidative Stress and Alterations of
648 BDNF and 5HT-3 Receptors of the Prefrontal Cortex in Female Rats. Neuropsychiatr Dis Treat 16:1777-1794.
649 Mowery TM, Kotak VC, Sanes DH (2015) Transient Hearing Loss Within a Critical Period Causes Persistent Changes
650 to Cellular Properties in Adult Auditory Cortex. Cereb Cortex 25:2083-2094.
651 Murthy S, Kane GA, Katchur NJ, Lara Mejia PS, Obiofuma G, Buschman TJ, McEwen BS, Gould E (2019) Perineuronal
652 Nets, Inhibitory Interneurons, and Anxiety-Related Ventral Hippocampal Neuronal Oscillations Are Altered
653 by Early Life Adversity. Biol Psychiatry 85:1011-1020.
654 Nocon JC, Gritton HJ, James NM, Mount RA, Qu Z, Han X, Sen K (2023) Parvalbumin neurons enhance temporal
655 coding and reduce cortical noise in complex auditory scenes. Commun Biol 6:751.
656 Ohashi K, Enomoto T, Joki Y, Shibata R, Ogura Y, Kataoka Y, Shimizu Y, Kambara T, Uemura Y, Yuasa D, Matsuo K,
657 Hayakawa S, Hiramatsu-Ito M, Murohara T, Ouchi N (2014) Neuron-derived neurotrophic factor functions as
658 a novel modulator that enhances endothelial cell function and revascularization processes. J Biol Chem
659 289:14132-14144.
660 Olah S, Fule M, Komlosi G, Varga C, Baldi R, Barzo P, Tamas G (2009) Regulation of cortical microcircuits by unitary
661 GABA-mediated volume transmission. Nature 461:1278-1281.
662 Overstreet-Wadiche L, McBain CJ (2015) Neurogliaform cells in cortical circuits. Nat Rev Neurosci 16:458-468.
663 Pan W, Pan J, Zhao Y, Zhang H, Tang J (2021) Serotonin Transporter Defect Disturbs Structure and Function of the
664 Auditory Cortex in Mice. Front Neurosci 15:749923.
665 Pardi MB, Schroeder A, Letzkus JJ (2023) Probing top-down information in neocortical layer 1. Trends Neurosci
666 46:20-31.

667 Pascual R, Zamora-Leon SP, Valero-Cabre A (2006) Effects of postweaning social isolation and re-socialization on
668 the expression of vasoactive intestinal peptide (VIP) and dendritic development in the medial prefrontal
669 cortex of the rat. Acta Neurobiol Exp (Wars) 66:7-14.

670 Pattwell SS, Bath KG (2017) Emotional learning, stress, and development: An ever-changing landscape shaped by
671 early-life experience. Neurobiol Learn Mem 143:36-48.

672 Perroud N, Zewdie S, Stenz L, Adouan W, Bavamian S, Prada P, Nicastro R, Hasler R, Nallet A, Piguet C, Paoloni-
673 Giacobino A, Aubry JM, Dayer A (2016) Methylation of Serotonin Receptor 3a in Adhd, Borderline
674 Personality, and Bipolar Disorders: Link with Severity of the Disorders and Childhood Maltreatment.
675 Depress Anxiety 33:45-55.

676 Pi HJ, Hangya B, Kvitsiani D, Sanders JI, Huang ZJ, Kepecs A (2013) Cortical interneurons that specialize in
677 disinhibitory control. Nature 503:521-524.

678 Poorthuis RB, Muhammad K, Wang M, Verhoog MB, Junek S, Wrana A, Mansvelder HD, Letzkus JJ (2018) Rapid
679 Neuromodulation of Layer 1 Interneurons in Human Neocortex. Cell Rep 23:951-958.

680 Poplawski J, Montina T, Metz GAS (2024) Early life stress shifts critical periods and causes precocious visual cortex
681 development. PLoS One 19:e0316384.

682 Priya R, Paredes MF, Karayannis T, Yusuf N, Liu X, Jaglin X, Graef I, Alvarez-Buylla A, Fishell G (2018) Activity
683 Regulates Cell Death within Cortical Interneurons through a Calcineurin-Dependent Mechanism. Cell Rep
684 22:1695-1709.

685 Pronneke A, Witte M, Mock M, Staiger JF (2020) Neuromodulation Leads to a Burst-Tonic Switch in a Subset of VIP
686 Neurons in Mouse Primary Somatosensory (Barrel) Cortex. Cereb Cortex 30:488-504.

687 Radtke-Schuller S, Schuller G, Angenstein F, Grosser OS, Goldschmidt J, Budinger E (2016) Brain atlas of the
688 Mongolian gerbil (Meriones unguiculatus) in CT/MRI-aided stereotaxic coordinates. Brain Struct Funct 221
689 Suppl 1:1-272.

690 Rajkumar R, Mahesh R (2010) The auspicious role of the 5-HT3 receptor in depression: a probable neuronal target? J
691 Psychopharmacol 24:455-469.

692 Rao D, Basura GJ, Roche J, Daniels S, Mancilla JG, Manis PB (2010) Hearing loss alters serotonergic modulation of
693 intrinsic excitability in auditory cortex. J Neurophysiol 104:2693-2703.

694 Rebello TJ, Yu Q, Goodfellow NM, Caffrey Cagliostro MK, Teissier A, Morelli E, Demireva EY, Chemiakine A,
695 Rosoklija GB, Dwork AJ, Lambe EK, Gingrich JA, Ansorge MS (2014) Postnatal day 2 to 11 constitutes a 5-HT-
696 sensitive period impacting adult mPFC function. J Neurosci 34:12379-12393.

697 Reh RK, Dias BG, Nelson CA, 3rd, Kaufer D, Werker JF, Kolb B, Levine JD, Hensch TK (2020) Critical period regulation
698 across multiple timescales. Proc Natl Acad Sci U S A 117:23242-23251.

699 Rikhye RV, Yildirim M, Hu M, Breton-Provencher V, Sur M (2021) Reliable Sensory Processing in Mouse Visual Cortex
700 through Cooperative Interactions between Somatostatin and Parvalbumin Interneurons. J Neurosci
701 41:8761-8778.

702 Rincon-Cortes M, Sullivan RM (2014) Early life trauma and attachment: immediate and enduring effects on
703 neurobehavioral and stress axis development. Front Endocrinol (Lausanne) 5:33.

704 Rosen MJ, Huyck JJ (2025) Hearing and early life adversity: effects of developmental stress on sensory processing.
705 Neuropsychopharmacology.

706 Schindelin J, Arganda-Carreras I, Frise E, Kaynig V, Longair M, Pietzsch T, Preibisch S, Rueden C, Saalfeld S, Schmid
707 B, Tinevez JY, White DJ, Hartenstein V, Eliceiri K, Tomancak P, Cardona A (2012) Fiji: an open-source
708 platform for biological-image analysis. Nat Methods 9:676-682.

709 Simpson KL, Weaver KJ, de Villers-Sidani E, Lu JY, Cai Z, Pang Y, Rodriguez-Porcel F, Paul IA, Merzenich M, Lin RC
710 (2011) Perinatal antidepressant exposure alters cortical network function in rodents. Proc Natl Acad Sci U S
711 A 108:18465-18470.

712 Stringer C, Wang T, Michaelos M, Pachitariu M (2021) Cellpose: a generalist algorithm for cellular segmentation. Nat
713 Methods 18:100-106.

714 Sunthimer MJ, Ye Y, Moore JT, White E, Snyder K, Mellott JG, Rosen MJ (2023) Interactions of Developmental
715 Stress and Hearing Loss on Gap Detection and the Auditory Cortex. 46th Midwinter Meeting of the
716 Association for Research:738-739.

717 Sweeney CG, Thomas ME, Liu CJ, Vattino LG, Smith KE, Takesian AE (2025) Reliable sensory processing of
718 superficial cortical interneurons is modulated by behavioral state. Cell Rep 44:115678.

719 Takatsuru Y, Koibuchi N (2015) Alteration of somatosensory response in adulthood by early life stress. Front Mol
720 Neurosci 8:15.

721 Takesian AE, Hensch TK (2013) Balancing plasticity/stability across brain development. Prog Brain Res 207:3-34.

722 Takesian AE, Bogart LJ, Lichtman JW, Hensch TK (2018) Inhibitory circuit gating of auditory critical-period plasticity.
723 Nat Neurosci 21:218-227.

724 Tierney TS, Moore DR (1997) Naturally occurring neuron death during postnatal development of the gerbil ventral
725 cochlear nucleus begins at the onset of hearing. J Comp Neurol 387:421-429.

726 Tsitsipa E, Rogers J, Casalotti S, Belessiotis-Richards C, Zubko O, Weil RS, Howard R, Bisby JA, Reeves S (2022)
727 Selective 5HT3 antagonists and sensory processing: a systematic review. Neuropsychopharmacology
728 47:880-890.

729 Vattino LG, Liu CJ, MacGregor CP, Sweeney CG, Minderler S, Takesian AE (2025) Primary auditory thalamus relays
730 directly to cortical layer 1 interneurons. iScience 28:112652.

731 Veenema AH (2009) Early life stress, the development of aggression and neuroendocrine and neurobiological
732 correlates: what can we learn from animal models? Front Neuroendocrinol 30:497-518.

733 Vitalis T, Parnavelas JG (2003) The role of serotonin in early cortical development. Dev Neurosci 25:245-256.

734 Wang Y, Gu Q, Cynader MS (1997) Blockade of serotonin-2C receptors by mesulergine reduces ocular dominance
735 plasticity in kitten visual cortex. Exp Brain Res 114:321-328.

736 Weikum WM, Oberlander TF, Hensch TK, Werker JF (2012) Prenatal exposure to antidepressants and depressed
737 maternal mood alter trajectory of infant speech perception. Proc Natl Acad Sci U S A 109 Suppl 2:17221-
738 17227.

739 Williams LE, Kuffer L, Bawa T, Husi E, Pages S, Holtmaat A (2025) Repetitive Sensory Stimulation Potentiates and
740 Recruits Sensory-Evoked Cortical Population Activity. J Neurosci 45.

741 Wong FK, Selten M, Roses-Novella C, Sreenivasan V, Pallas-Bazarra N, Serafeimidou-Pouliou E, Hanusz-Godoy A,
742 Oozeer F, Edwards R, Marin O (2022) Serotonergic regulation of bipolar cell survival in the developing
743 cerebral cortex. Cell Rep 40:111037.

744 Yajima H, Haijima A, Khairinisa MA, Shimokawa N, Amano I, Takatsuru Y (2018) Early-life stress induces cognitive
745 disorder in middle-aged mice. Neurobiol Aging 64:139-146.

746 Yarden TS, Mizrahi A, Nelken I (2022) Context-Dependent Inhibitory Control of Stimulus-Specific Adaptation. J
747 Neurosci 42:4629-4651.

748 Ye Y, Mattingly MM, Sunthimer MJ, Gay JD, Rosen MJ (2023) Early-Life Stress Impairs Perception and Neural
749 Encoding of Rapid Signals in the Auditory Pathway. J Neurosci 43:3232-3244.

750 Zhang C, Zhu H, Ni Z, Xin Q, Zhou T, Wu R, Gao G, Gao Z, Ma H, Li H, He M, Zhang J, Cheng H, Hu H (2022) Dynamics
751 of a disinhibitory prefrontal microcircuit in controlling social competition. Neuron 110:516-531 e516.

752 Zhu Y, Qiao W, Liu K, Zhong H, Yao H (2015) Control of response reliability by parvalbumin-expressing interneurons
753 in visual cortex. Nat Commun 6:6802.

754 Zolfaghari FS, Pirri F, Gauvin E, Peeri M, Amiri S (2021) Exercise and fluoxetine treatment during adolescence
755 protect against early life stress-induced behavioral abnormalities in adult rats. Pharmacol Biochem Behav
756 205:173190.

757